Advanced 3D Monte Carlo Algorithms for Biophotonic and Medical Applications

Lewis McMillan

University of
St Andrews

This thesis is submitted in partial fulfillment for the degree of
PhD
at the
University of St Andrews

August 2019

Declaration

I, Lewis McMillan, hereby certify that this thesis, which is approximately 34067 words in length, has been written by me, that it is the record of work carried out by me, or principally by myself in collaboration with others as acknowledged, and that it has not been submitted in any previous application for a higher degree.

I was admitted as a research student in September 2015 and as a candidate for the degree of PhD in September 2015; the higher study for which this is a record was carried out in the University of St Andrews between 2015 and 2019.

Date ..... Signature of candidate .....

I hereby certify that the candidate has fulfilled the conditions of the Resolution and Regulations appropriate for the degree of PhD in the University of St Andrews and that the candidate is qualified to submit this thesis in application for that degree.

Date ..... Signature of supervisor .....

Date ..... Signature of supervisor .....

Abstract

The Monte Carlo radiation transfer (MCRT) method can simulate the transport of light through turbid media. MCRT allows the simulation of multiple anisotropic scattering events, as well as a range of microphysics such as polarisation, and fluorescence. This thesis concerns the development of several MCRT algorithms to solve various biophotonic and medical problems. Modelling of tissue ablation, autofluorescent signals, and a theoretical quasi-wave/particle MCRT model were developed as part of this thesis.

Tissue ablation can be used to treat acne scarring and Rhinophyma, it can also be used to help enhance topical drug delivery. Currently depth of ablation is not easily elucidated from a given laser or laser power setting. Therefore, a numerical tissue ablation model is developed using MCRT, a heat diffusion model, and a numerical tissue damage model to assess ablation crater depth and thermal damage to the surrounding tissue.

Autofluorescence is the natural fluorescence of biological structures in tissue. Autofluorescence can be used as a biomarker of several diseases including: cardiovascular diseases, Alzheimers and diabetes. However, the origin of the signal is not completely clear. The effect of tissue optics on the signal, which fluorophores contribute to the signal and by how much, and how different locations on the body can effect the signal are all not well understood. This thesis presents a study of the effect of tissue optics on the autofluorescent signal. As part of this study AmoebaMCRT was created to determine the relative concentrations of fluorophores for a given autofluorescent signal.

Finally, we developed an extension to the MCRT method that allows the simulation of quasi-wave/particles. This method relies on the Huygens-Fresnel principle and the tracking of the phase of each individual photon packet. The extension, φMC, allows the modelling of complex beams that require the wave properties of light such as arbitrary order Bessel beams, and Gaussian beams. We then use φMC to predict which beam, Bessel or Gaussian, preforms "better" in a highly turbid medium.

Acknowledgements

Contents

List of Figures

Appendices

Appendix A

Fresnel Reflections

In order to be able to accurately model the paths that light take in a medium where the refractive indices vary, Fresnel reflections and refractions must be modelled. To model these reflections and refractions in a simulation we calculate the Fresnel coefficients. Equations (A.1) to (A.3) show the equations for calculating these for s and p* polarised light, and unpolarised light (Eq. (A.3)).

$$R_s = \left| \frac{n_1 \cos\theta_i - n_2 \cos\theta_t}{n_1 \cos\theta_i + n_2 \cos\theta_t} \right|^2 \tag{A.1}$$

$$R_p = \left| \frac{n_1 \cos\theta_t - n_2 \cos\theta_i}{n_1 \cos\theta_t + n_2 \cos\theta_i} \right|^2 \tag{A.2}$$

$$R_{eff} = \tfrac{1}{2}\left(R_s + R_p\right) \tag{A.3}$$

Where:
θ_i and θ_t are the angle of incidence and angle of transmission respectively,
see Eqs. (A.4) and (A.5) and Figs. A.1 and A.2;
n_1 and n_2 are the refractive indices of the current medium and the transmission medium [-];
R_s and R_p are the reflectance coefficients for s and p polarised light respectively [-];
finally, R_{eff} is the effective reflective coefficient for unpolarised light [-].

$$\sin\theta_t = \frac{n_1}{n_2}\sin\theta_i \tag{A.4}$$

$$\cos\theta_t = \sqrt{1. - \sin\theta_t{}^2} \tag{A.5}$$

R_{eff} gives the probability of reflection or refraction for a ray of light with an angle of incidence θ_i.

To calculate the angles of reflection and refraction, a vector form of Snell's law is used. Using the geometry illustrated in Fig. A.1 one can see that:

$$I = A + B \tag{A.6}$$

$$R = A - B \tag{A.7}$$

*s and p polarised light is senkrecht (German for perpendicular), and parallel with respect to the electric field of the light and the pane of an interface.

$$B = \cos(\theta) \cdot N \tag{A.8}$$

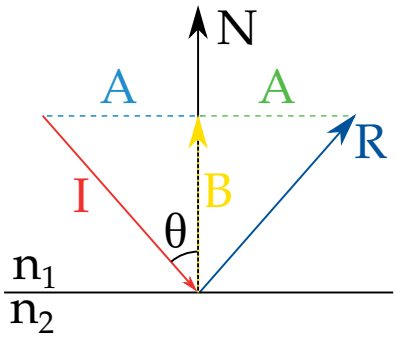

Figure A.1: *Geometry for reflection of light at a refractive change boundary. I is incident light direction vector, R is the reflected light, and N is a normal to the surface. Here, θ is the angle of incidence which is equal to the angle of reflection.*

Therefore, substituting Eq. (A.8) into Eqs. (A.6) and (A.7) and rearranging yields:

$$I = A + \cos(\theta) \cdot N \tag{A.9}$$
$$R = A - \cos(\theta) \cdot N \tag{A.10}$$

$$\therefore R = I - 2(N \cdot I)N \tag{A.11}$$

Where R gives the vector for a ray of light that has undergone reflection. Next we treat the transmission case. Figure A.2 gives the geometry for the situation, where the circle is a unit circle.

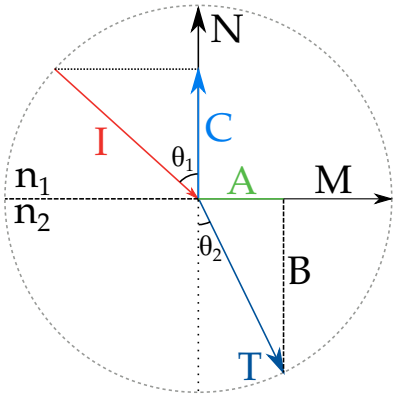

Figure A.2: *Geometry of light refraction and reflections.*

Again, one can deduce the following using trigonometry and Fig. A.2:

$$T = A + B \tag{A.12}$$
$$A = \sin(\theta_2)\, M \tag{A.13}$$
$$B = \cos(\theta_2)\,(-N) \tag{A.14}$$
$$C = \cos(\theta_1)\, N \tag{A.15}$$
$$M = \frac{I + C}{\sin(\theta_1)} \tag{A.16}$$

Substituting Eqs. (A.13) to (A.16) into Eq. (A.12), using Snell's law (Eq. (A.21)), and rearranging yields:

$$T = A + B \tag{A.17}$$
$$= M \sin\theta_2 - N\cos\theta_2 \tag{A.18}$$
$$= \frac{I + C}{\sin\theta_1}\sin\theta_2 - N\cos\theta_2 \tag{A.19}$$
$$= \frac{(I + \cos\theta_1 N)\sin\theta_2}{\sin\theta_1} - N\cos\theta_2 \tag{A.20}$$
$$\frac{\sin\theta_1}{\sin\theta_2} = \frac{\eta_1}{\eta_2} \tag{A.21}$$
$$\therefore T = \frac{\eta_1}{\eta_2}(I + \cos\theta_1 N) - N\cos\theta_2 \tag{A.22}$$
$$T = \eta + (\eta c_1 - c_2)\, N \tag{A.23}$$

Where Eq. (A.22) can be simplified to Eq. (A.23) by defining the following expressions:

$$c_1 = N \cdot I \tag{A.24}$$
$$c_2 = \sqrt{1. - \eta^2(1. - c_1^2)} \tag{A.25}$$
$$\eta = \frac{\eta_1}{\eta_2} \tag{A.26}$$

To apply Eqs. (A.11) and (A.23) to our voxel model, the algorithm checks if there is a change in refractive index whenever a photon packet moves into a new voxel. If there is a change of refractive index the packet is placed on the surface of the voxel, and the algorithm calculates the surface normal of the voxel the light has hit and uses the above equations to calculate R_{eff}. With R_{eff} calculated a random number, ξ, is drawn. If ξ is less than R_{eff} then the photon packet is reflected, otherwise then the packet is refracted into the new voxel. The new direction vectors are set according to Eqs. (A.11) and (A.23), a new optical depth is generated, and the packet is propagated as normal.

Appendix B

Detected Light Fluence Tracking Method

Most of the fluence graphs presented in this thesis show the fluence of the incident light throughout the simulated medium. However, there are problems where tracking the fluence of the detected light maybe useful, though this quantity is not straight forward to track. The current method of tracking fluence is to add pathlengths, calculated as the packet moves from voxel to voxel to a 3D array. This method obviously cannot determine which packet will be detected before the packet is detected, therefore a new method must be devised. This new method tracks the coordinates, direction vectors, random optical distance and fluorescent source of the packet using a stack. A stack is a commonly used abstract data structure, and is a collection of elements. In this case the elements are the coordinates, direction vectors, optical distance and fluorescent source. A stack has two main operations, pop and push. The push operation adds a new element to the collection, and the pop operation removes the most recently added element from the collection. This is known as last in first out (LIFO). Figure B.1 shows these two operations in action.

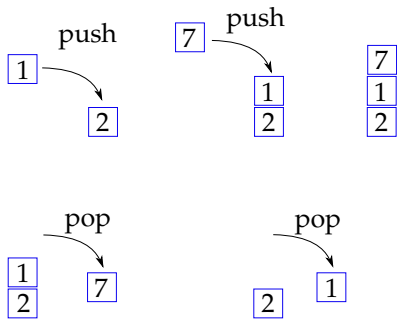

Figure B.1: *Example of the push and pop operation on a stack. The first operation adds the integer 2 to the stack. The second operation pushes 7 to the stack. The last operation pops the 7 from the stack.*

The progress of each packet is pushed onto the stack, as it is propagated through the simulated medium. As mentioned above the packet's coordinates, direction vectors, optical depth, and fluorescent source are the quantities pushed to the stack. These quantities are pushed to stack

every time an interaction event occurs. When a packet is terminated, either via absorption or it leaving the medium, the packets details are removed from the stack. This occurs unless the packet is detected. If the packet is detected then the information remains on the stack. This whole process repeats until all the packets have been run. Once all the packets have been run, the packets are "replayed". This is achieved by popping the information off the stack and passed to the inttau2 routine. The packet is the propagated again, this time recording the fluence as done in most of the chapters in this thesis.

Appendix C

Spectra from Tissue Optics Study

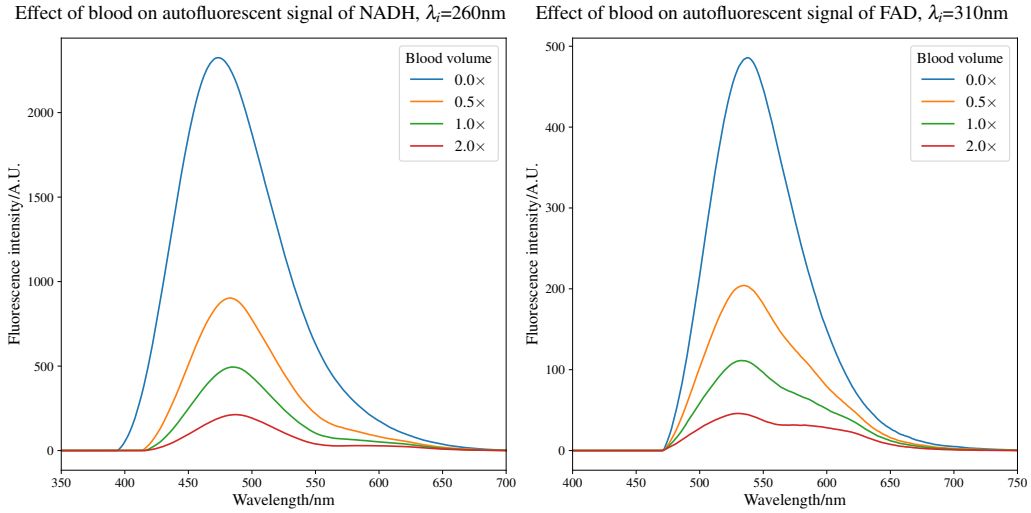

Figure C.1: *Effect of blood content on NADH (left) and FAD (right) autofluorescence.*

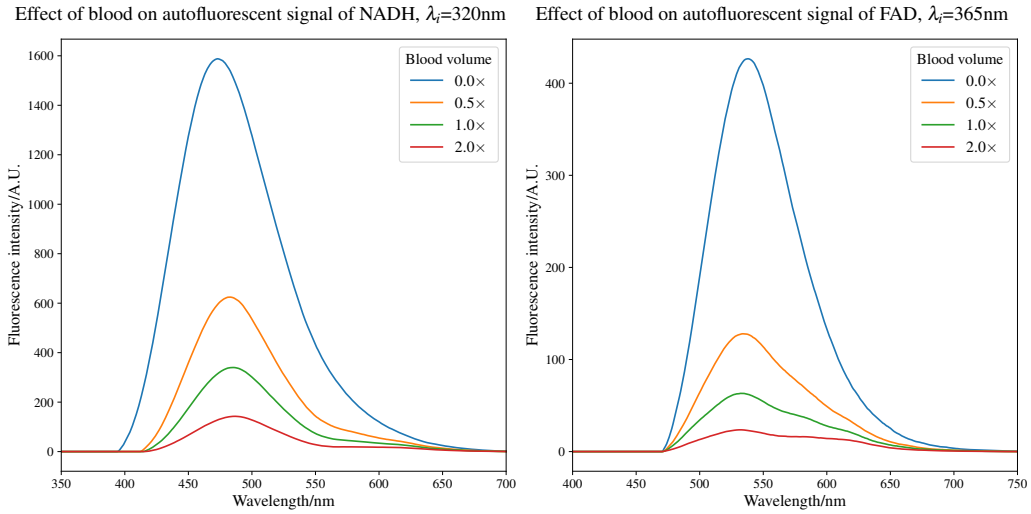

Figure C.2: *Effect of blood content on NADH (left) and FAD (right) autofluorescence.*

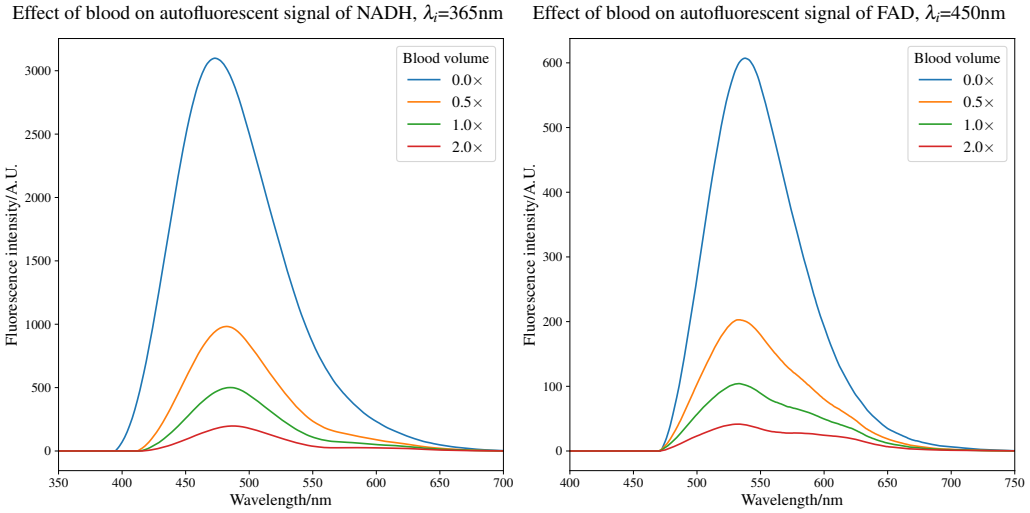

Figure C.3: *Effect of blood content on NADH (left) and FAD (right) autofluorescence.*

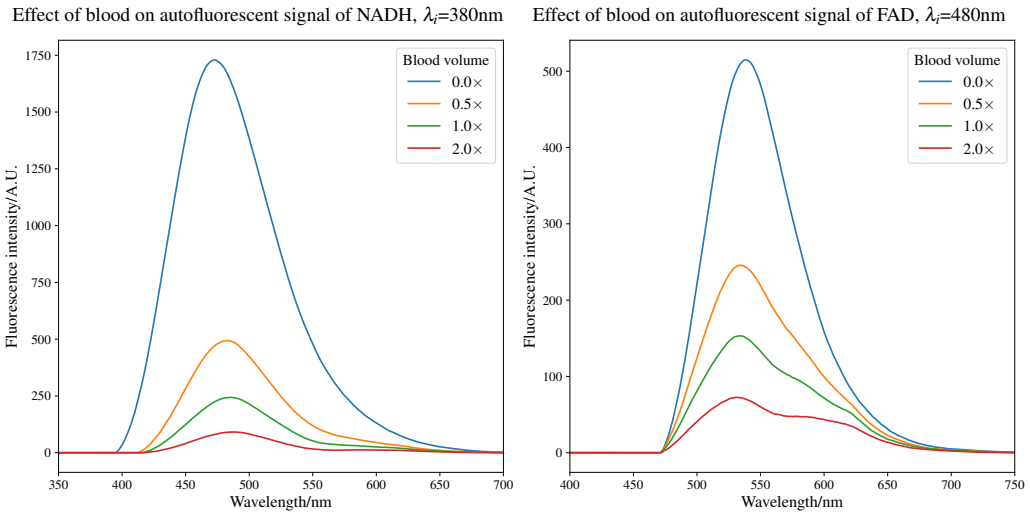

Figure C.4: *Effect of blood content on NADH (left) and FAD (right) autofluorescence.*

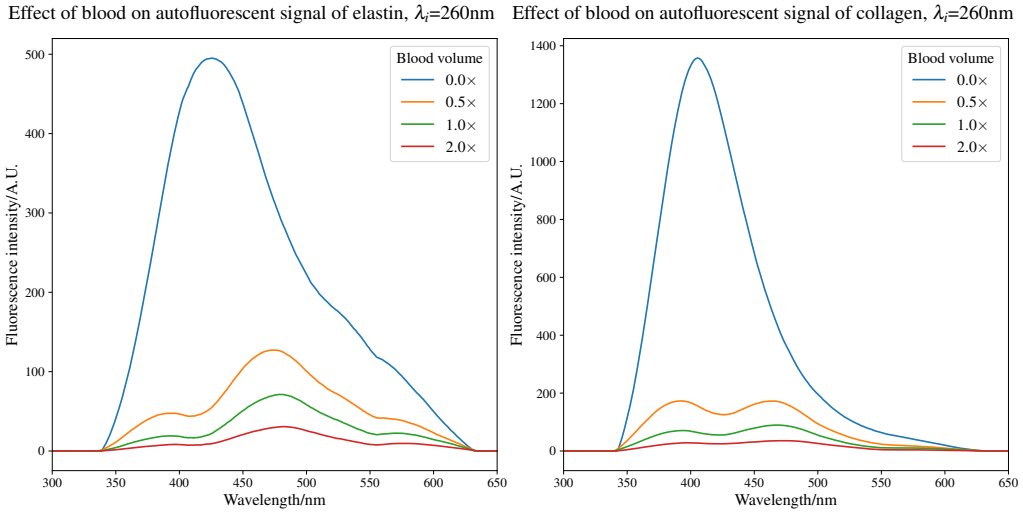

Figure C.5: *Effect of blood content on elastin (left) and collagen (right) autofluorescence.*

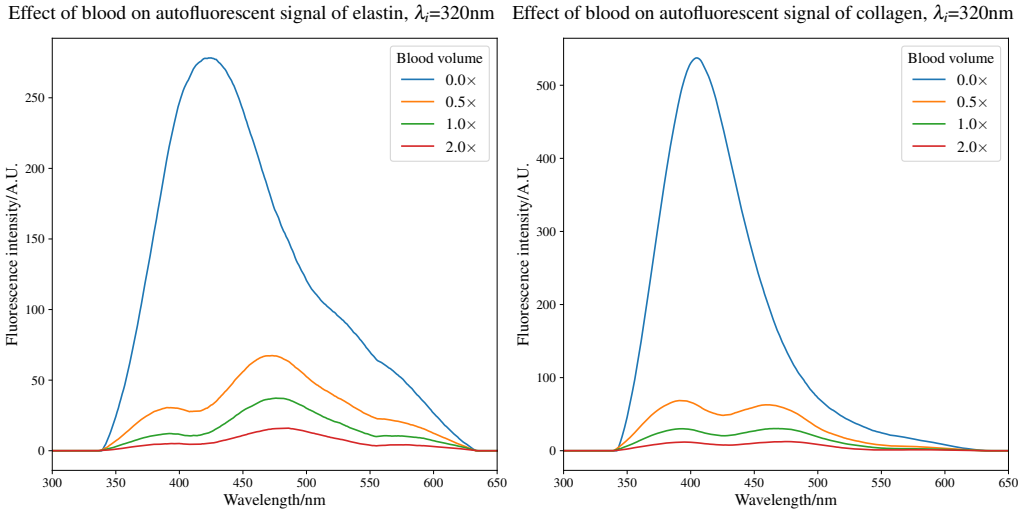

Figure C.6: *Effect of blood content on elastin (left) and collagen (right) autofluorescence.*

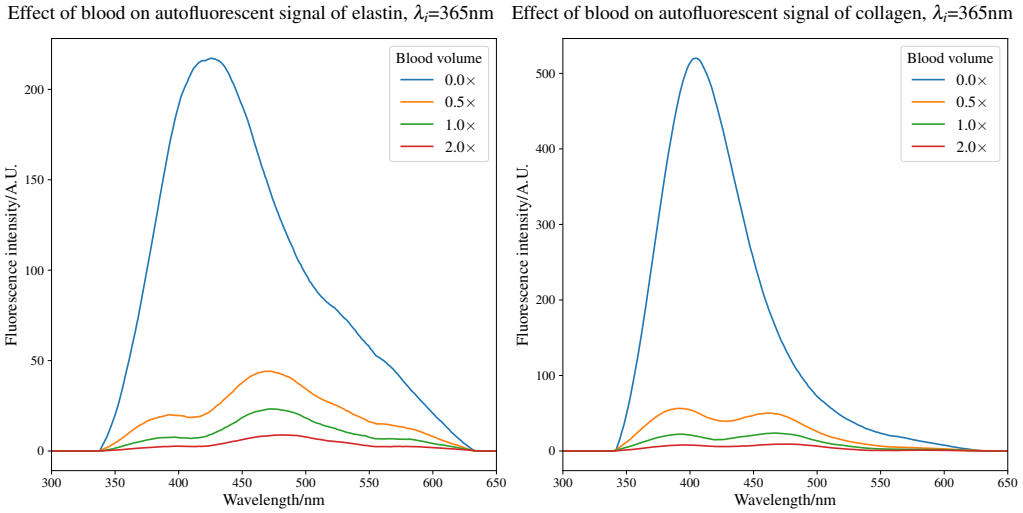

Figure C.7: *Effect of blood content on elastin (left) and collagen (right) autofluorescence.*

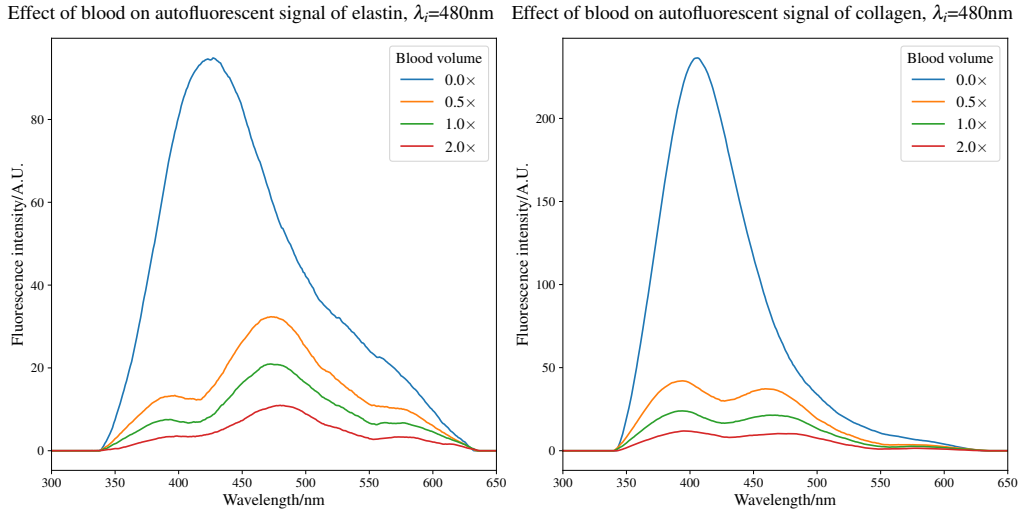

Figure C.8: *Effect of blood content on elastin (left) and collagen (right) autofluorescence.*

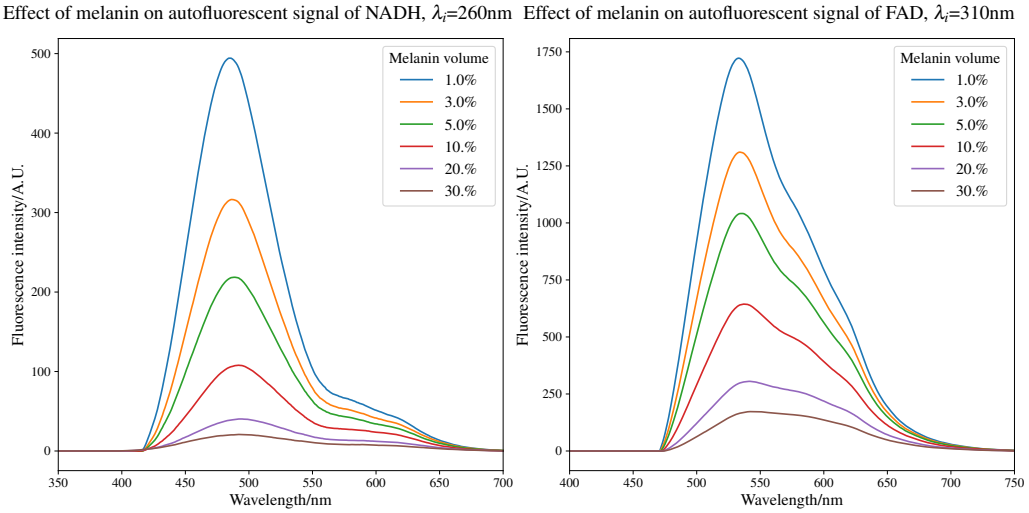

Figure C.9: *Effect of melanin content on NADH (left) and FAD (right) autofluorescence.*

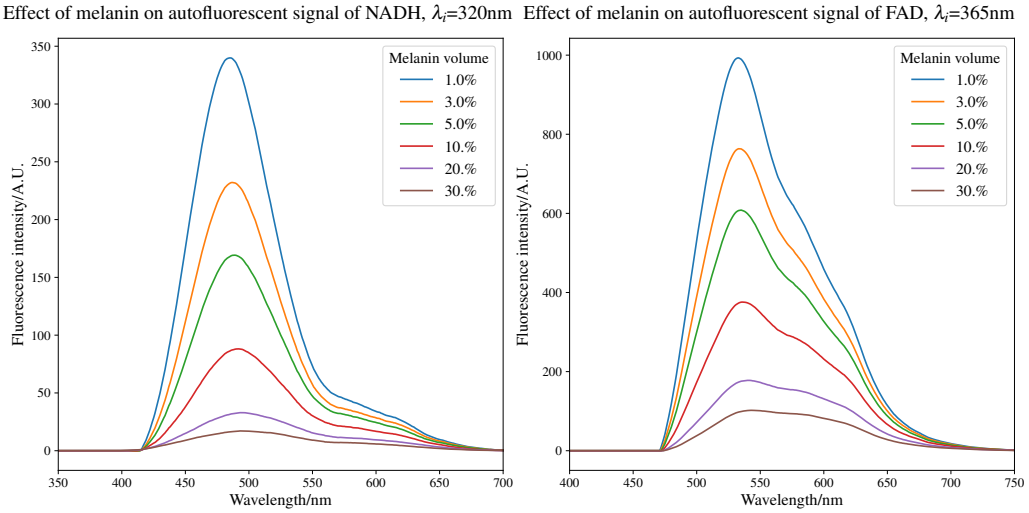

Figure C.10: *Effect of melanin content on NADH (left) and FAD (right) autofluorescence.*

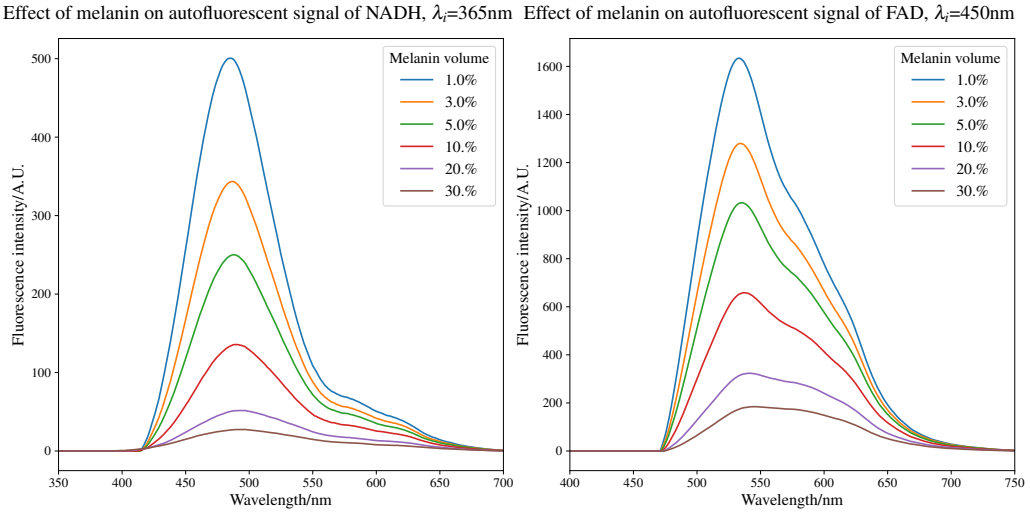

Figure C.11: *Effect of melanin content on NADH (left) and FAD (right) autofluorescence.*

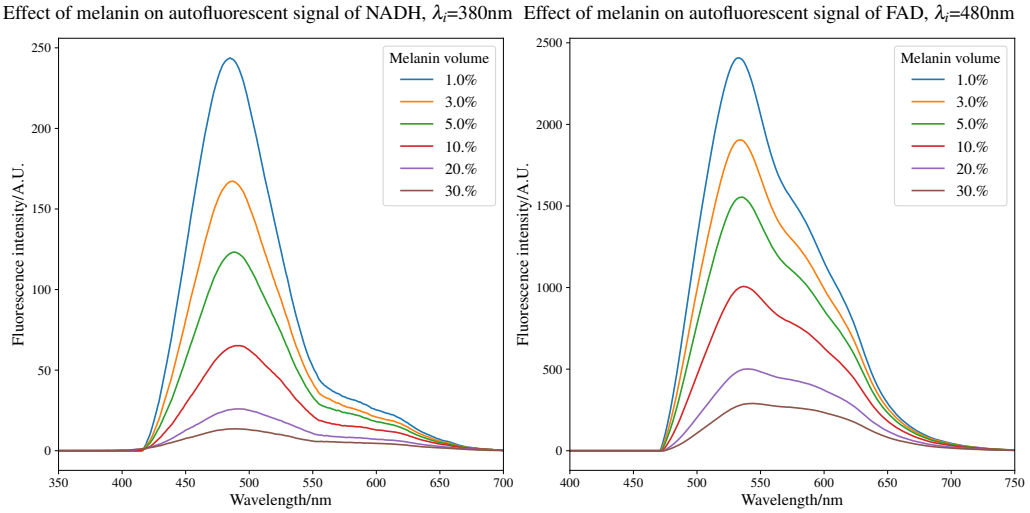

Figure C.12: *Effect of melanin content on NADH (left) and FAD (right) autofluorescence.*

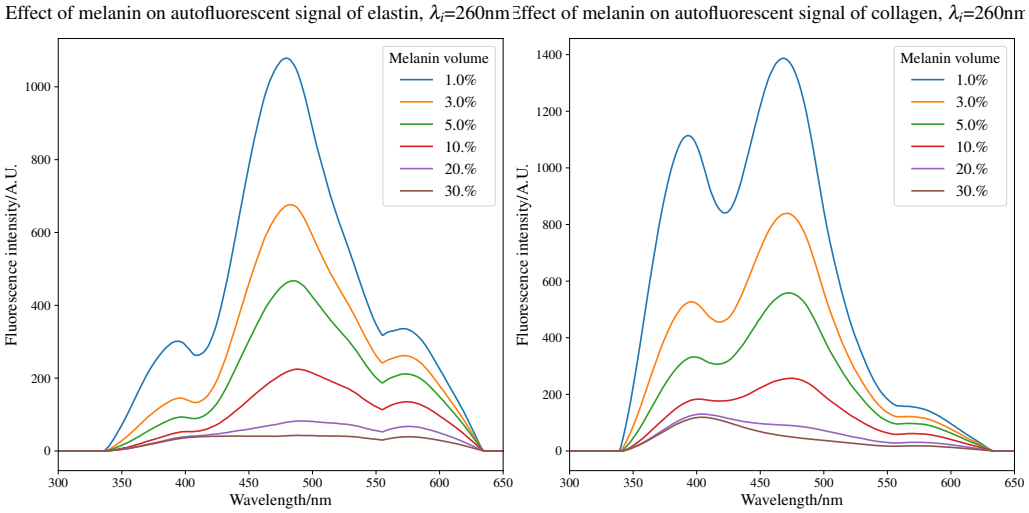

Figure C.13: *Effect of melanin content on elastin (left) and collagen (right) autofluorescence.*

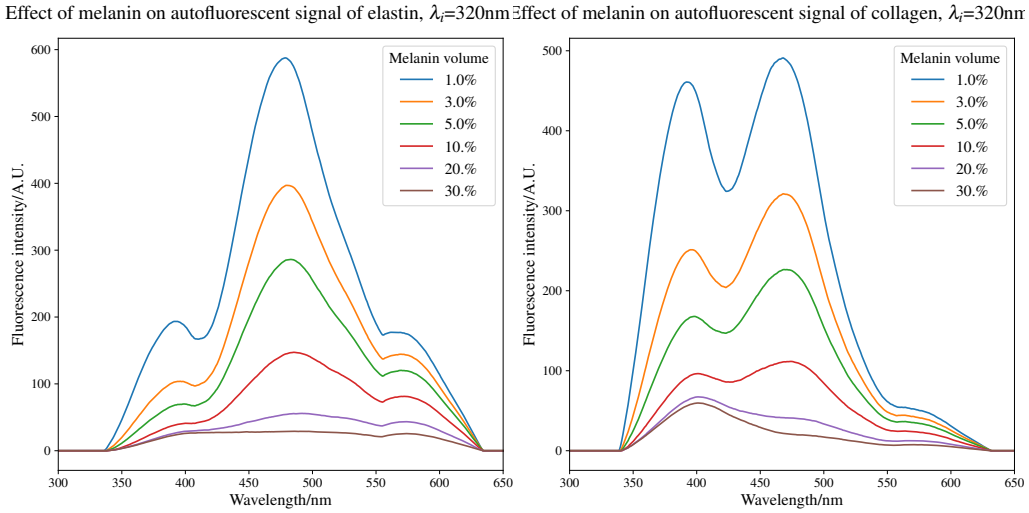

Figure C.14: *Effect of melanin content on elastin (left) and collagen (right) autofluorescence.*

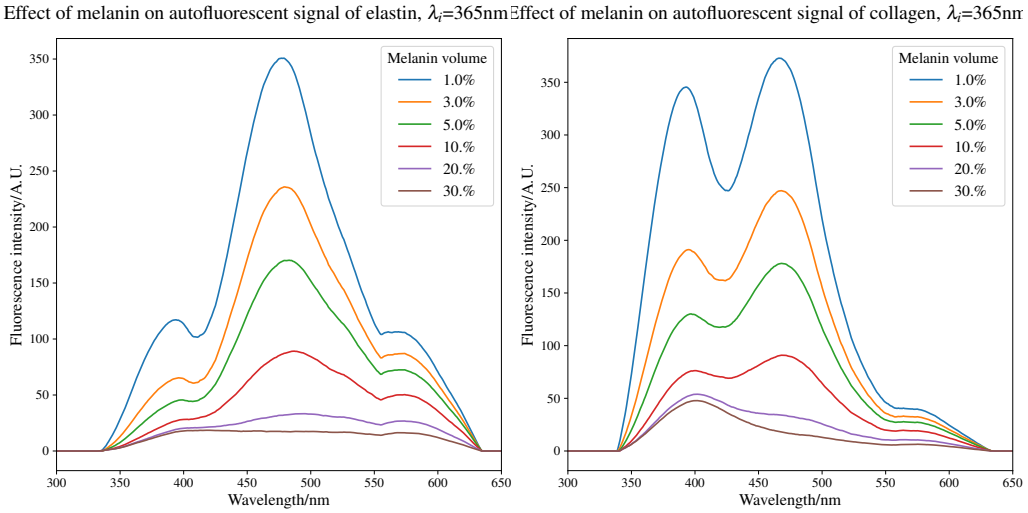

Figure C.15: *Effect of melanin content on elastin (left) and collagen (right) autofluorescence.*

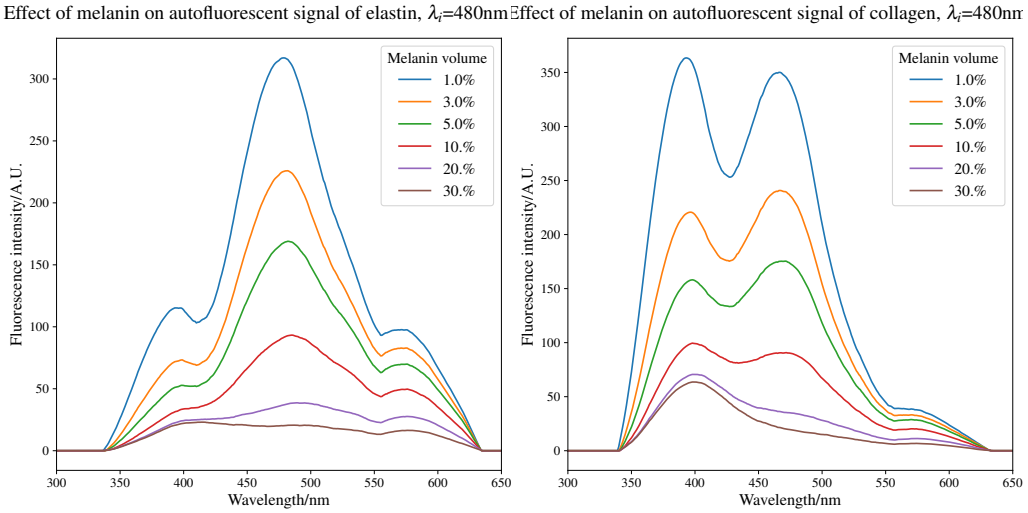

Figure C.16: *Effect of melanin content on elastin (left) and collagen (right) autofluorescence.*

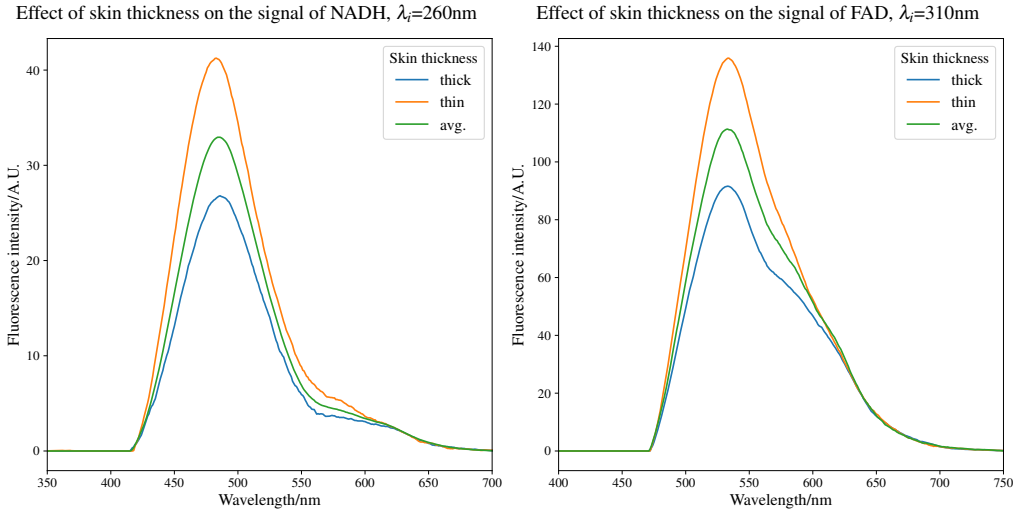

Figure C.17: *Effect of skin thickness content on NADH (left) and FAD (right) autofluorescence.*

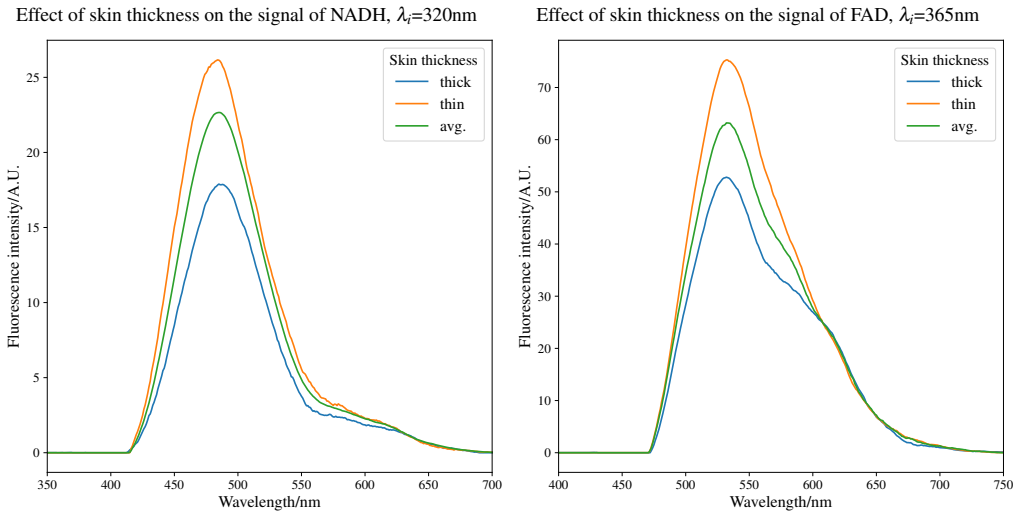

Figure C.18: *Effect of skin thickness content on NADH (left) and FAD (right) autofluorescence.*

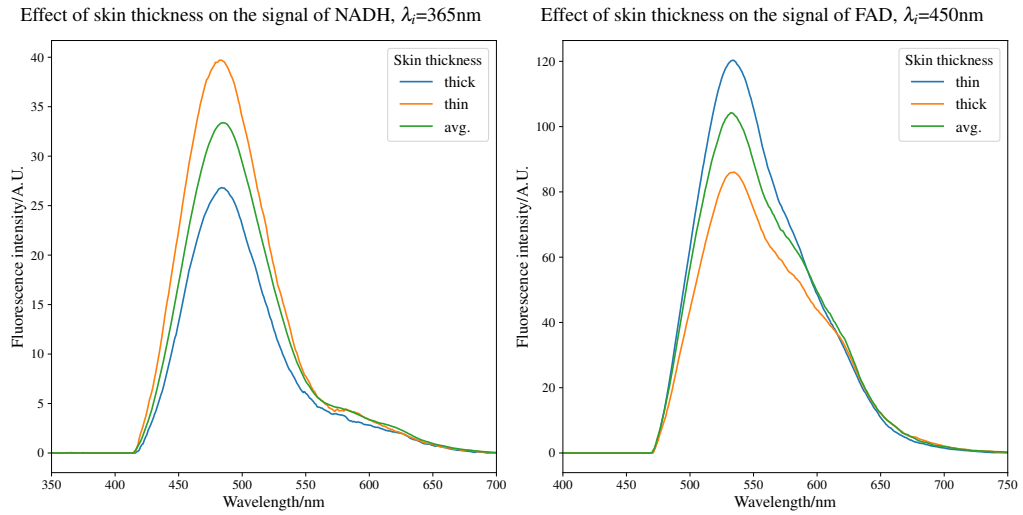

Figure C.19: *Effect of skin thickness content on NADH (left) and FAD (right) autofluorescence.*

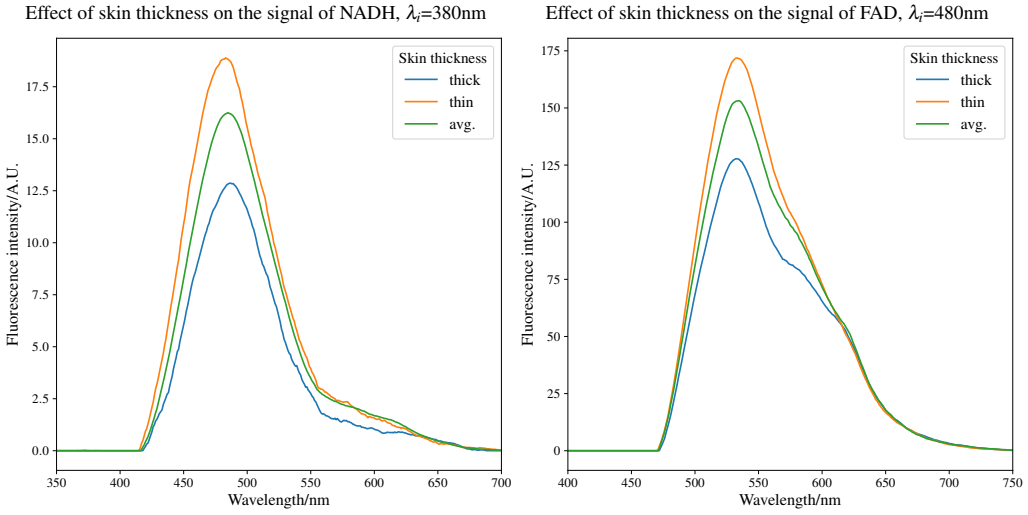

Figure C.20: *Effect of skin thickness content on NADH (left) and FAD (right) autofluorescence.*

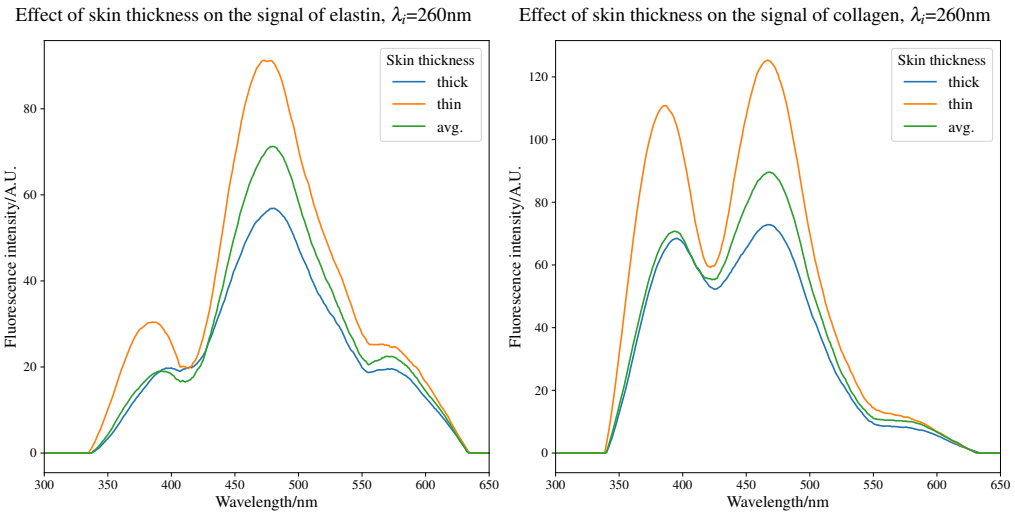

Figure C.21: *Effect of skin thickness content on elastin (left) and collagen (right) autofluorescence.*

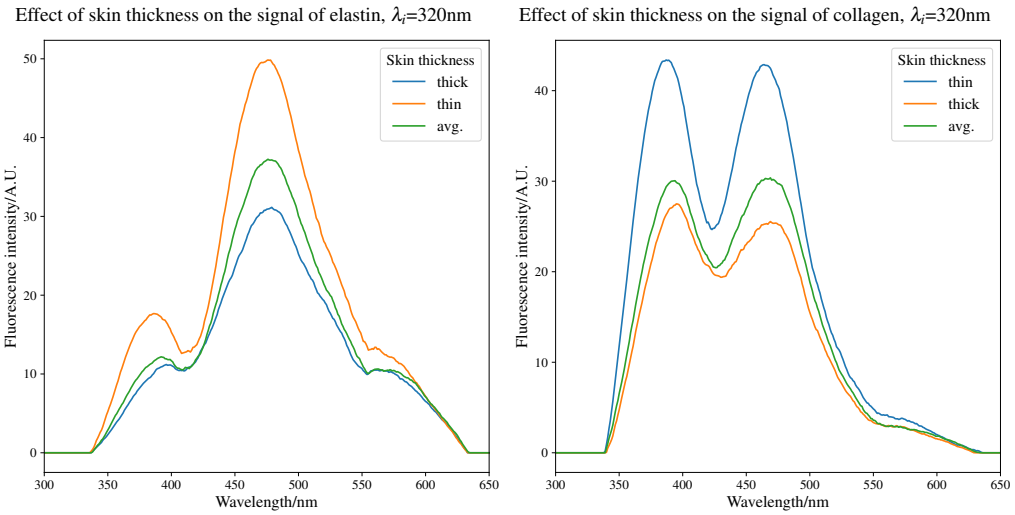

Figure C.22: *Effect of skin thickness content on elastin (left) and collagen (right) autofluorescence.*

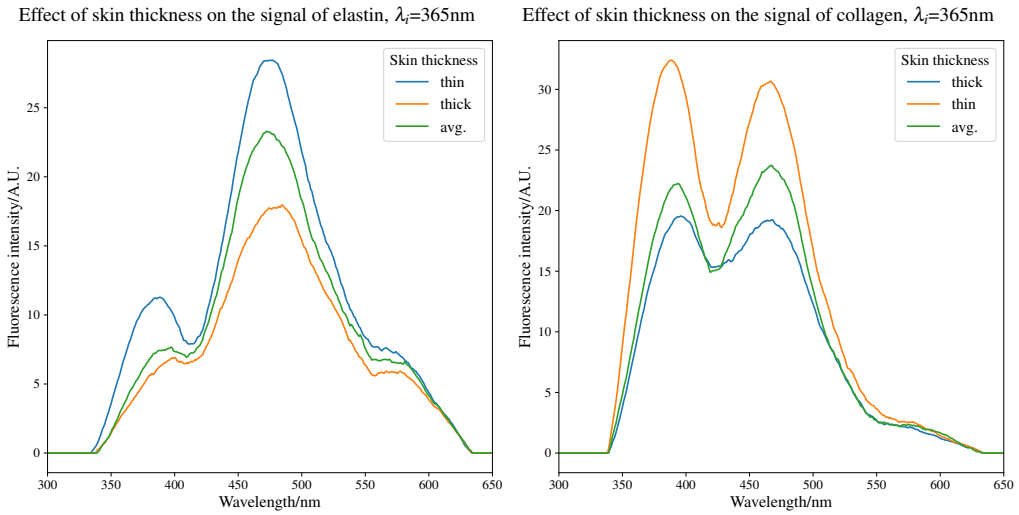

Figure C.23: *Effect of skin thickness content on elastin (left) and collagen (right) autofluorescence.*

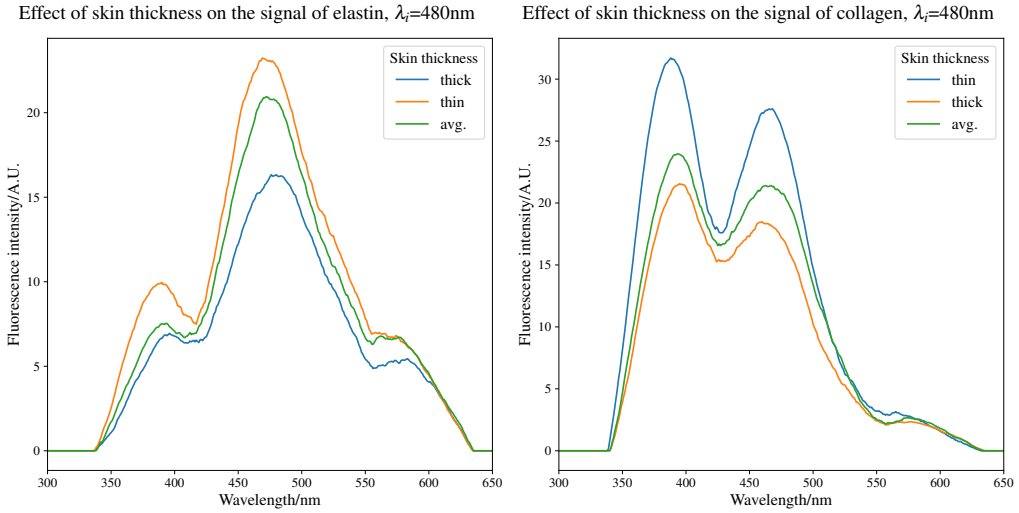

Figure C.24: *Effect of skin thickness content on elastin (left) and collagen (right) autofluorescence.*

Bibliography